Effect of supercooling on the microstructural development and optimization of physical properties of melt grown SnSe crystals

A. G. Kunjomana[1] · J. Bibin[1] · R. Karthikeyan[1] · S. Varadharajaperumal[2]

Abstract

The microstructural development of stoichiometric tin monoselenide (SnSe) crystals grown by vertical Bridgman–Stockbarger method using an indigenously fabricated furnace has been investigated under high vacuum ($\sim 10^{-6}$ mbar). The ampoule translation rate (t_r) and supercooling, ΔT ($= T_m - T$, where T_m is the melting point and T is the crystallization temperature) were varied in the range, 12–2 mm/h and 20–100 °C respectively. Enhancement of ΔT and t_r led to constitutional supercooling, inducing compositional changes and non-stoichiometry. Low ΔT (20–40 °C) and high t_r (12–10 mm/h) resulted in globules, flakes and cavities. When $\Delta T = 60$ °C and $t_r = 9$ to 7 mm/h, mounds were formed with closed contours and ripples, due to atomically rough liquid–solid (l-β) interface. Fine tuning of ΔT (60 °C) and t_r (2 mm/h) enabled smooth planar interface, so as to yield good quality crystalline structures with periodic atomic deposition promoting crystal growth, layer-by-layer. Energy dispersive analysis by X-rays and powder X-ray diffraction studies revealed appreciable crystallinity, chemical homogeneity and phase purity. The density of crystals estimated from crystallographic data (6.183 g/cm^3) corroborates with that obtained utilizing Archimedes principle. Thermogravimetric and microindentation analyses established thermal and mechanical stability. The low etch pit density ($\sim 10^2$ cm^{-2}) manifests nearly perfect growth of crystals than their melt counterparts. UV–Vis–NIR and PL spectra reflected direct transition with an energy gap of 1.32 eV, validating immense potential of the grown crystals for photovoltaic applications.

1 Introduction

The scientific advancement of crystal growth has achieved major breakthroughs in the development of proficient crystals with enhanced performance for optoelectronic applications. Despite the tremendous progress that has been witnessed in science and technology, there remain challenges to architect crystalline samples with regard to the complexities in the material perspectives and thermodynamics involved with the control of a phase change [1, 2]. The choice of a substance is influenced by dissociability, chemical reactivity, thermal stability, melting point, polymorphism, etc. The structure–property relationship, therefore, governs the device performance as the polycrystalline aggregates are inferior to single crystals. There is a dearth of information to make use of reliable cost-effective materials, which are efficient compared to the expensive counterparts for the direct conversion of solar into electrical energy [3, 4]. Solar energy sector is still in a nascent stage and hence systematic work is to be executed for tailoring novel properties with the aid of a viable synthesis process. In this regard, compound semiconductors undoubtedly play a vital role to provide good quality layers with versatile optical characteristics in addition to high mechanical strength and stability, under a controlled atmosphere. In an eco-friendly approach, tin monoselenide stands apart as a sustainable material owing to its optimum energy gap (1.30 eV), high absorption coefficient and non-hazardous nature. Due to the demerits of the elemental semiconductor, silicon, such as indirect transition and high refinement costs [5, 6], SnSe has gained wide attraction as a promising candidate of the IV–VI chalcogenide family for the fabrication of photovoltaic structures [7, 8], due to its exemplary properties and tunability. This compound is to be synthesized in the form of bulk crystals for bringing out unique behaviour so as to meet the industrial requirements. Crystal growth can be understood in wide sense as

✉ A. G. Kunjomana
kunjomana.ag@christuniversity.in

1 Department of Physics and Electronics, CHRIST (Deemed to be University), Bangalore, Karnataka 560 029, India

2 Centre for Nano Science and Engineering (CeNSE), Indian Institute of Science (IISc), Bangalore, Karnataka 560 012, India

an excellent scientific procedure to control phase transitions that lead to the creation of single crystalline solids with well-defined symmetry. Natural crystals are scarce and the existing ones are not superior enough to provide desired characteristics for fulfilling the functionality of devices. So, the artificial synthesis of pure and stoichiometric samples with good crystallinity is imperative to cater to the rapidly growing industrial demand, as they form the core of material engineering applications. Advanced techniques like liquid phase epitaxy (LPE), vapour phase epitaxy (VPE), metalorganic chemical vapour deposition (MOCVD), atomic-layer epitaxy (ALE), chemical vapour transport (CVT), chemical bath deposition (CBD), chemical vapour deposition (CVD), electrodeposition, etc. are expensive, involve several complicated reactions and induce extraneous traces of particles, contamination, precipitates, oxides, by-products, etc. Therefore, these methods are not practically feasible for large scale production. Structural defects or stacking faults were also associated in the deposited samples [9–13]. Although solution and chemical vapour growth routes are alternate approaches, the grown structures are prone to adverse effects caused by foreign elemental contamination and non-stoichiometry that inhibit perfection [14, 15]. Liu et al. [16] reported that the analysis of imperfections is of technological importance for enhancing the device characteristics. It is thus necessary to develop a facile, robust and relatively safe, yet less costly method for harvesting the products, tailoring the growth conditions. Of all various growth processes, Bridgman–Stockbarger method is versatile, simple and efficient, owing to its ease of use, effectiveness and advantages such as the synthesis of bulk crystalline samples with controlled diameter, density and high yield, devoid of facets or impurity striations. This method is commonly employed for the production of GaSe, Bi_2Te_3, Sb_2Te_3, InSb, and GaTe semiconductors for electronic devices [2]. Though this technique is not suitable for materials which decompose before melting, it is highly applicable for those which melt congruently without segregation. Hence, we report for the first time, the systematic pathways for the microstructural development of SnSe crystals in a controlled environment with optimization of synthesis protocols so as to promote their internal lattice perfection, stoichiometry and properties towards optoelectronic applications.

2 Materials and methods

The complexities involved in the device performance are primarily associated with the intrinsic attributes of materials, but can be reduced by the advances in fabrication technology. Commercially procured precursors are highly expensive, and possess undesirable foreign elements that are detrimental to the desired functionality, if used as the host nutrient for crystal growth. Presence of inorganic impurities in the ampoule greatly increases the probability of multiple nucleation sites, which leads to polymorphism. The intricacies of chemical dynamics hinder the liquid–solid phase transitions, which in turn induce defects in the grown crystals. In the drive towards greener and efficient processes, material engineering using home-made instrumentation was employed to artificially harvest good quality products using stoichiometric SnSe precursor in an economically viable manner. Utmost care was taken to ensure the homogeneity of the samples free from contamination. Grease and dust in the procured tubes were removed with soap solution and distilled water followed by sulphuric acid treatment. After subjecting to ultrasonic waves, fine traces of impurities in the ampoule were eliminated by nitrogen plasma treatment. High pure (99.999%) Sn and Se were weighed in the ideal atomic proportion of SnSe (50.00:50.00 at.%), sealed under high vacuum $\sim 10^{-6}$ mbar and kept in a muffle furnace maintained at a temperature of 920 °C. The pre-reaction of the constituent elements was made possible by rotating the ampoule at the rate of 60 rpm periodically for 48 h using a specially assembled rotation mechanism, with the aid of a dynaflux synchronous motor. After stabilizing the thermal conditions utilizing a dimmerstat voltage controller, chromel–alumel thermocouple and mechanical relay, slow cooling was done at the rate of 2 °C/min. The obtained SnSe compound was close to the standard stoichiometric composition with the elemental ratio, Sn:Se = 50.01:49.99 at.%. This chemically homogeneous charge was powdered and filled in a quartz ampoule (length 150 mm and inner diameter 15 mm) with a tapered tip for favouring the growth from a single site. For growth, the melt temperature was held maximum at 920 °C in a customized Bridgman-Stockbarger furnace integrated with a programmable microprocessor-based temperature controlling system. Supercooling at the tip of the ampoule was varied systematically, so as to optimize the driving force for bulk crystallization. Experimental trials were systematically executed to explore the microstructural development during the unidirectional solidification, subjecting to t_r = 12–2 mm/h with the aid of an in-house-fabricated translation mechanism. The vacuum sealed ampoule was kept in the stabilized hot zone of the furnace. In each growth run, the ampoule containing the molten liquid was lowered relative to the furnace at constant growth velocity (t_r) to the cold zone. Globules and flake like structures were observed under low supercooling ($\Delta T \leq 20$ °C), whereas compositional changes leading to non-stoichiometry occurred due to constitutional supercooling ($\Delta T \geq 100$ °C). Special attention was therefore given to inhibit the dissociated/decomposed state of the molten liquid near the melting point, in order to avoid segregation of elements, while exploring the pathways from $\Delta T = 20$ to 100 °C. Under the growth conditions, $\Delta T = 60$ °C and $t_r = 2$ mm/h, the crystals were found to exhibit superior

quality with novel characteristics. The harvested products were removed from the ampoules and polished in deionized water to eliminate any residual contaminants. The physically distinct and chemically homogeneous samples were cleaved under liquid nitrogen to minimize deformations and probed using various techniques. Inverted metallurgical (Metagraph-I) and scanning electron (ULTRA 55) microscopes were employed in the present work, as these tools are the most beneficial and fundamental to investigate the morphology, grain size, structure and microstructural studies of the samples. ASTM E112 grain size measurement was executed using the horizontal intercept method, which is coupled with the optical microscope. Microindentation analysis was carried out at room temperature, utilizing the Vickers microhardness tester (MVH-I) in the load range of 10–100 g at a dwell time of 15 s and the hardness values were computed with the help of Quantimet software. Composition of the cleaved crystals was assessed by energy dispersive analysis by X-rays (EDAX). The phase identification and evaluation of structural parameters have been made possible with the aid of powder X-ray diffractometer (Rigaku SmartLab). The diffraction profiles were recorded over the 2θ range 10–80° with the step size of 0.02°. Thermogravimetric analysis was done using Perkin Elmer instrument to assess the thermal stability and crystallization behavior of the samples in the range 27–1000 °C. Fluorolog-3 spectrometer with a steady-state excitation source of 450 W xenon arc lamp was utilized to record the photoluminescence (PL) profile of the samples. Optical absorption properties were also investigated by a UV–Vis–NIR spectrophotometer (Varian, Cary 5000) for exploring the suitability of samples with regard to photovoltaic applications.

3 Results and discussion

3.1 Growth of SnSe crystals using an indigenously tailored stoichiometric precursor

The inherent properties of a crystal profoundly depend upon its internal structure, distribution of defects or irregularities, which in turn are governed by the growth kinetics associated with the propagation of liquid–solid (l-β) interface. The mode of transition from the molten liquid to solid is influenced by the heat flow dynamics during melt growth, under varying temperature at constant pressure [17, 18]. The factors involved in controlled solidification comprise three basic steps: achievement of supercooling, formation of stable nucleus and its successive growth to yield macroscopic size [19, 20]. Hence, microstructural development of SnSe crystals has been investigated based on the synthesis conditions [1]. Quality of the grown samples depends upon the atomically smooth, rough or diffused nature of the interface as depicted in Fig. 1a–d [21]. That is, the level of supercooling, $\Delta T = T_m - T$, becomes the driving force for melt growth. The thermodynamic kinetic factor, Gibbs free energy is given by

$$G = H - TS, \qquad (1)$$

where S is the entropy, which is lowest for a nearly perfect crystal grown in a closed system due to energy exchange with its surroundings [1]. The most stable state of a system is that which possesses the minimum Gibbs free energy [22].

The free energy change (ΔG) during the transformation of molten liquid (l) to a crystal (β) is depicted in Fig. 1e. Below T_m, the free energy of the latter is lower than the former and crystallization takes place spontaneously as $\Delta G = G_\beta - G_l < 0$ (criterion for stability of a periodic solid). The difference in the Gibbs free energy for the l-β transition is expressed as

$$\Delta G = \Delta V\,\Delta P - \Delta S\,\Delta T, \qquad (2)$$

where ΔP and ΔT ($= T_m - T$) show the deviation from the equilibrium values. For melt growth at constant pressure (ΔP = 0) [1],

$$\Delta G = -\Delta S\,\Delta T = -\Delta H\,\Delta T/T_m, \qquad (3)$$

where ΔH denotes the change in enthalpy, which is released during crystallization. Negative sign indicates the decrease in internal energy during the transformations between the lower crystallographic and higher non-crystallographic microstates of the system. Such transformations are of utmost importance to exploit the mechanism of solidification for fine tuning the quality of the harvested products. When ΔT increases with decrease in crystallization temperature, supercooling exceeds the critical free energy, ΔG* such that the thermodynamic drive enables the building blocks to approach each other with the release of latent heat due to exothermic process so as to accomplish bulk crystals, once a stable critical nucleus is formed [20].

In the present work, the nature of solid surfaces was investigated as per the above thermodynamic conditions with the aid of optical and SEM images. The principle of Bridgman–Stockbarger method is such that the nutrient substance is melted in a container with a pointed tip (Fig. 1f) and lowered to cold zone (Fig. 2), so that crystallization embarks on, to form a primary stable embryo [2, 23]. As mentioned above, successful growth will be facilitated only with the decrease in free energy. But, the problem of crystal growth is nucleation control as it involves precise solidification of a melt in order to promote the extension of a single nucleus without giving rise to new nuclei. In this regard, melt growth of chalcogenide compounds such as CdTe, PbTe, ZnSe, etc. was discussed in the literature [24–27]. Nevertheless, the reports were elusive with regard to the microstructural development, growth mechanism, defect control and optimization of stoichiometric composition. Although the crystal growth of such binary semiconductors
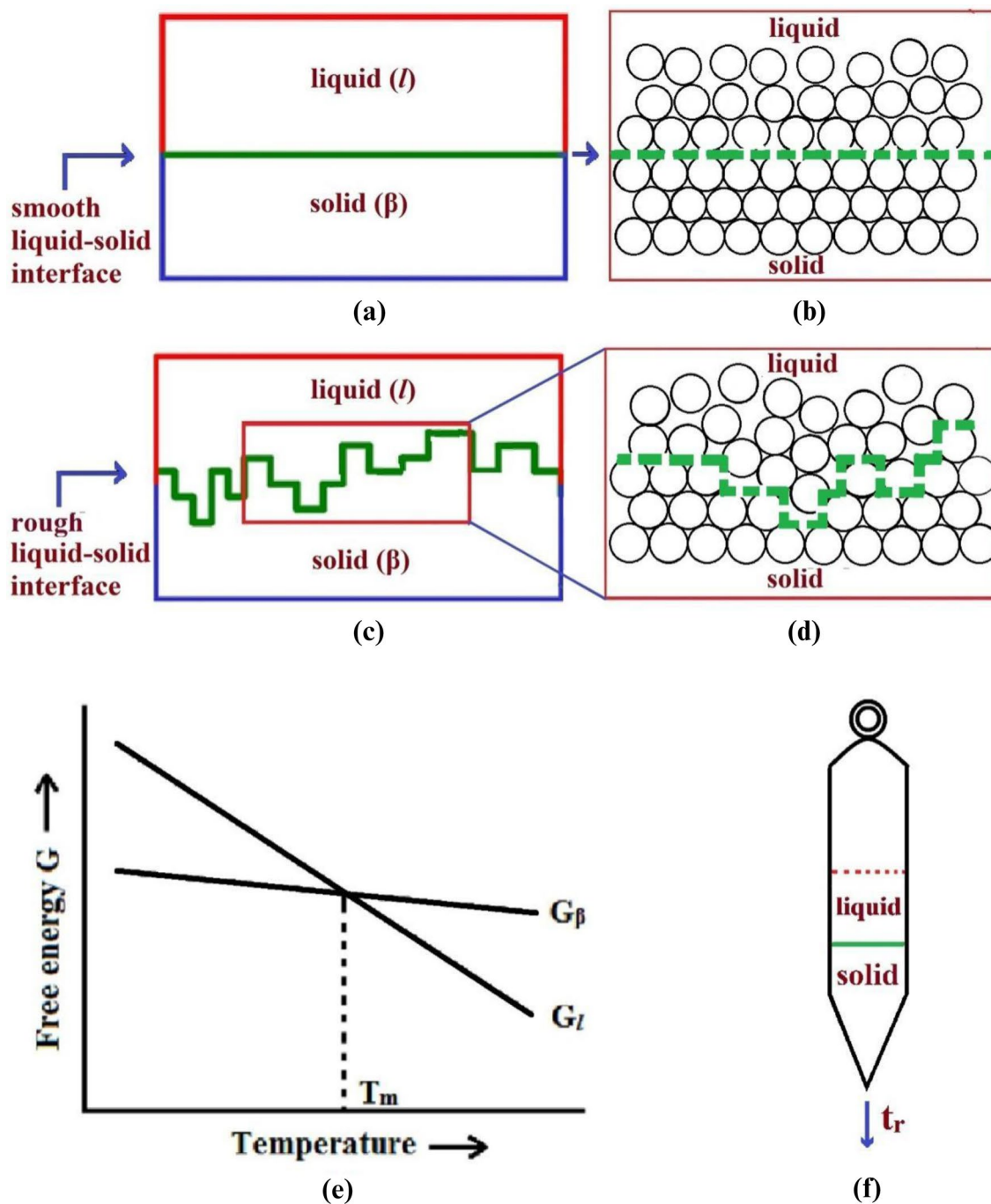
Fig. 1 Liquid–solid interfaces: **a**, **b** atomically smooth, **c**, **d** atomically rough [21], **e** free energy versus temperature plot for the liquid and solid phases [22] and **f** schematic of a tapered ampoule employed for Bridgman–Stockbarger method [2]

was discussed, the microstructural development of SnSe crystals has not been explored so far. Hence, we tackled the challenges by investigating the effect of supercooling of tin monoselenide in the range, $\Delta T = 20$ to $100\ ^\circ C$ by maintaining $t_r = 12–2$ mm/h (Table 1). For each growth run, the crystallization temperature and growth velocity were stabilized using a translation assembly (motor–gear system) integrated

with a programmable temperature controlling mechanism as shown in Fig. 2.

For crystallization in melt growth, heat transfer plays a critical role and the difference in density between the liquid and solid phases is lesser (Fig. 1b, d) compared to vapour or solution growth processes [19]. The green dotted lines (Fig. 1b, d) show the very same region as that in Fig. 1a and
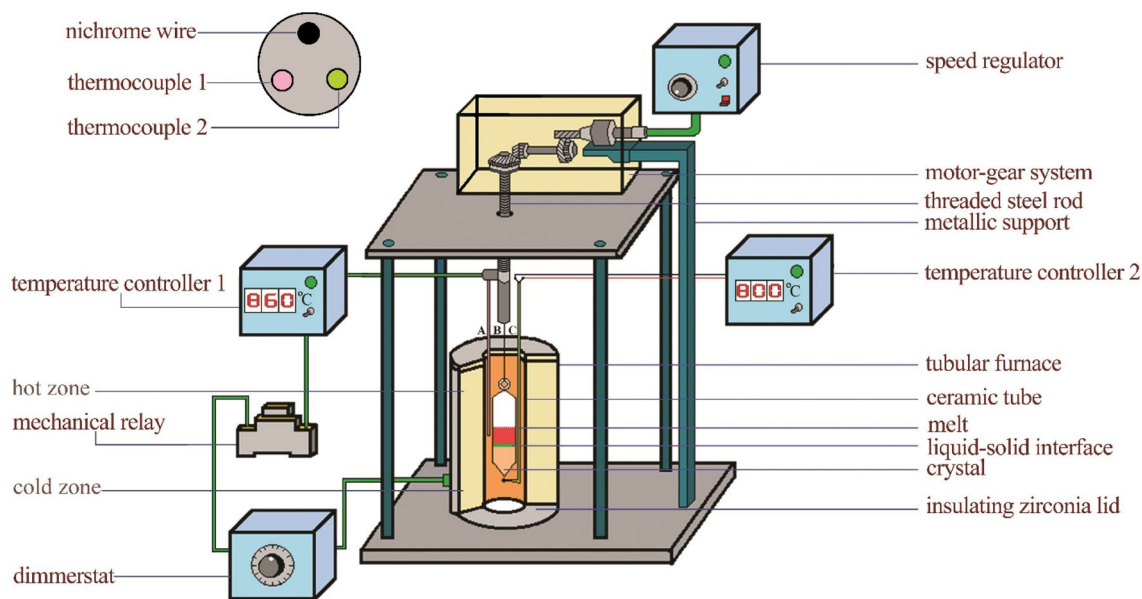
Fig. 2 Schematic of the home-made experimental set up utilized for crystal growth

Table 1 SnSe crystals grown under different growth conditions

Temperature (°C)		t_r (mm/h)	ΔT (°C)	Microstructural development of SnSe crystals
T_m	T			
860	840	12	20	Globules and flakes (Fig. 3a)
860	820	11	40	Origin of deep cavities (Fig. 4a)
860	820	10	40	Emergence of shallow cavities (Fig. 4b)
860	800	9	60	Mounds with contours (Fig. 5a)
860	800	8	60	Mound with closed loops (Fig. 5b)
860	800	7	60	Mound with spread of growth layers (Fig. 5c)
860	800	6	60	Ramped structure without mounds (Fig. 6a)
860	800	5	60	Grains with nearly parallel layers (Fig. 6c)
860	800	4	60	Formation of flat growth steps (Fig. 7a)
860	800	3	60	Layer-by-layer growth (Fig. 7c)
860	800	2	60	Crystals with smooth surface (Fig. 8a)
860	780	2	80	Onset of polycrystallinity (Fig. 8b)
860	760	2	100	Atomically rough surface (Fig. 8c)

c respectively, manifesting the separation between the aperiodic bonding in the liquid atoms and the strong interatomic packing in the crystal structure [19, 21]. When the crystallization temperature was close to the melting point, i.e. $T_m − T = 860–840$ °C ($\Delta T = 20$ °C), the grain structure showed the formation of multiple nuclei due to discrete growth centers at random sites in the tip of ampoule as a result of thermal shock under a faster translation rate of 12 mm/h. Crystals were grown due to irregular packing of solid particles as displayed in Fig. 3a associated with the rapid transition from liquid to solid over several atomic layers in accordance with Fig. 1c or d, causing disorder across the interface with high entropy. Rough interfaces are also referred as diffused or

non-faceted as the transformation is interface controlled in melt growth [21]. Owing to the turbulent heat flow near the interface, the atoms in the condensed phase will have more freedom of movement, inducing the solid phase under thermal stress and experience high disorder and entropy. During the non-equilibrium process associated with the movement of liquid–solid interface, solid nuclei are not always likely to be stable as they are created and destroyed by the random motion of the liquid particles continuously with increase in internal energy. Spurious nucleation and the resultant formation of polycrystals occur due to irregular rate of deposition in the boundary layer, disrupting periodicity of the sample. Globules and flakes were thus observed under high
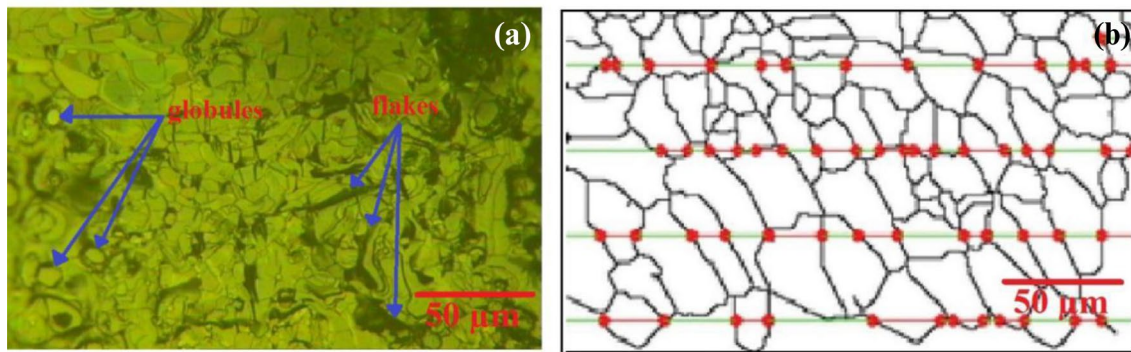
Fig. 3 **a** Optical image showing globules and flakes in crystals grown under the conditions, $\Delta T = 20$ °C and $t_r = 12$ mm/h and **b** grain size evaluation [29]

crystallization temperature as depicted in Fig. 3a. But there were no signs of dendritic or spherulitic growth induced by the instability of the growth front as observed in the Bridgman growth of GaSe [28]. When T = 840 °C, the tip of the ampoule offered multiple heterogeneous sites, generating polycrystalline rather than single crystal growth due to the atomically rough interface. Thus, increased number of grains with uneven size disrupting the flatness as marked in Fig. 3a arose, due to high nucleation density. As discussed by Teena and Kunjomana [29], the average grain size was computed as 7.61 μm, based on the scale bar (Fig. 3b) provided by the Quantimet image analyzer integrated with a metallurgical microscope. Nucleation, growth and ripening are complicated processes and exhibit stochastic behaviour even in ultrasonically cleaned quartz ampoules, due to the factors such as surface roughness, particle size distribution, thermal history, etc. as reported by Málek et al. [30] in supercooled melt and spherulitic crystals.

Hence, to inhibit the perturbing nucleation process and the subsequent unstable deposition under high growth temperature and velocity, the transfer of atoms across the interface during solidification was controlled so as to promote the evolution of polycrystalline to smooth morphology. For this purpose, it is imperative to reduce the translation rate slowly and stabilize the crystallization zone at a lesser temperature. When T = 820 °C ($\Delta T = 40$ °C, and $t_r = 11$ mm/h) the crystallites increased in size, but cavities originated (Fig. 4a) due to lack of periodic localization of atoms under high internal energy, limiting the quality of crystals. Hence, the translation rate was intentionally reduced to 10 mm/h (Fig. 4b), fostering particle diffusion and adsorption to attain the equilibrium solid state. Polycrystalline structures grew with the coalescence of grains bearing volume defects (voids) due to the inadequacy of material supply while cooling.

Structural imperfections were minimized and crystal ripening was made nearly perfect by enhancing periodic atomic addition of the host charge for the evolution of bulk crystals. For this purpose, the translation rate and crystallization temperature were carefully tailored. With increase in ΔT
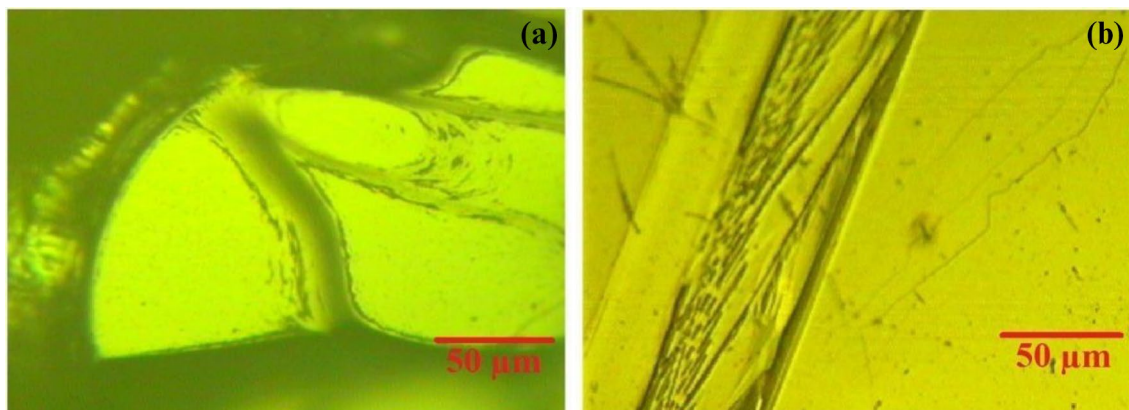

Fig. 4 Optical images depicting cavities in crystals grown under the conditions: **a** $\Delta T = 40$ °C and $t_r = 11$ mm/h and **b** $\Delta T = 40$ °C and $t_r = 10$ mm/h

(= 60 °C) by stabilizing temperature, T (= 800 °C), the hollow space was filled within the grains due to adequate supply of solute concentration, after the stable nucleus is formed. However, contours and ripples were detected microscopically due to diffused interface arising out of morphological instabilities at t_r = 9 mm/h and 8 mm/h (Fig. 5a, b) rather than accomplishing atomically flat crystal surface as per the theoretical considerations [1, 30]. Stress field in the lattice was caused due to hopping of atoms in the crystallization front. Thus, mounds with propagation of contours, ripples and kinks were observed as depicted in Fig. 5a–c. The piling of dislocated steps arises under the influence of thermal stress produced in the sample related to the constraining of the neighbouring lattice regions. In this case, heterogeneous nucleation originates due to structural irregularities like micro-inhomogeneities [31]. Over deposition and spreading of growth steps from such active growth sites are clearly seen in Fig. 5. It is well known that the crystal quality for device application is profoundly influenced by the structural irregularities during the process of crystal growth. Hence, morphological stability was facilitated with regard to slow movement of interface, by setting t_r = 7 mm/h. Degree of atomic ordering was fairly enhanced and resulted in the lateral advance of nearly parallel growth steps rather than

closed rings, due to the expansion of loops, as evidently seen in Fig. 5c. Although the steps straighten from the kinks, the persistence of wavy nature near the imperfections prevails due to the asymmetry of atomic attachment.

When t_r was set to 6 mm/h, progressive crystal growth was facilitated due to periodic atom-by-atom arrangement and resulted in the absence of cracks, mounds, ripples, etc. Nevertheless, the crystalline structure was ramped (Fig. 6a), as the initiation of flat interface was limited owing to the anisotropy in directional solidification. The generation of steps and kinks were detected microscopically due to the propagation of faceted interface. The development of crystalline growth pattern shown in this figure can be vividly related in terms of the schematic model (Fig. 6b), where the atoms are represented as cubes for analogy. The undesirable growth conditions caused the surface not to be perfectly planar, because the atoms entered to the terrace, migrated in a disordered fashion and irregularly adsorbed to the kink sites due to entropy such that the crystal growth proceeded with irregular movement of kinks and the advancement of steps.

Therefore, to improve the crystallinity, subsequent trials were performed by deliberately reducing the translation rate to 5 mm/h, such that well-defined layers were tangentially deposited in each grain as portrayed in Fig. 6c.
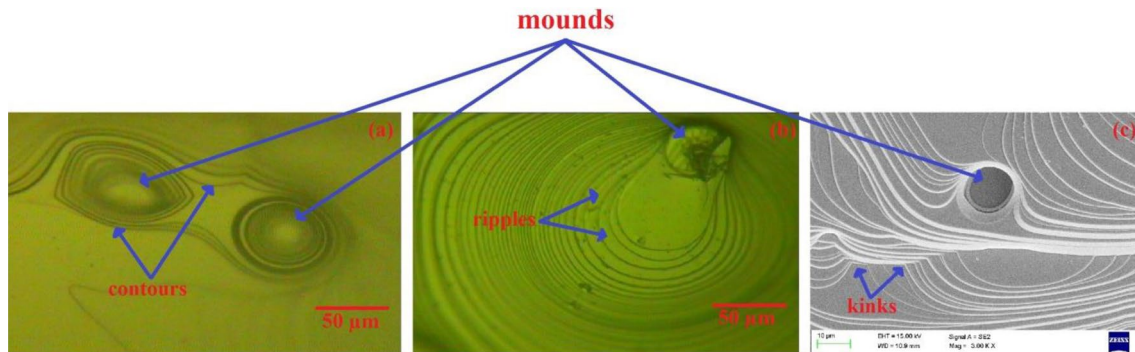
Fig. 5 Micrographs of crystals exhibiting mounds with contours, ripples and kinks grown under the conditions: **a** ΔT = 60 °C and t_r = 9 mm/h, **b** ΔT = 60 °C and t_r = 8 mm/h and **c** ΔT = 60 °C and t_r = 7 mm/h
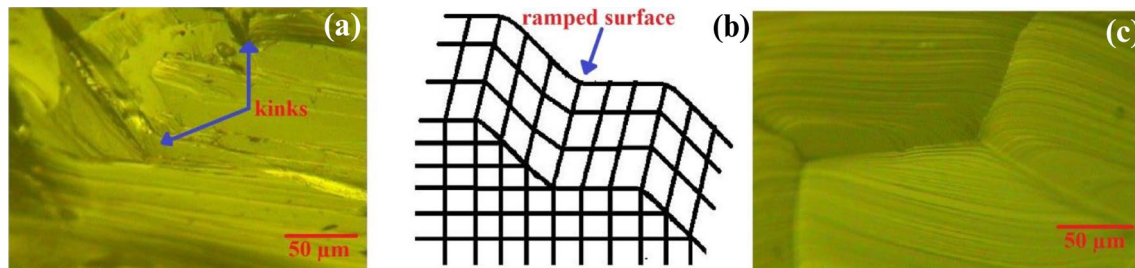
Fig. 6 **a** Optical image of a crystal grown under the condition, ΔT = 60 °C and t_r = 6 mm/h, **b** atomic model showing a sloping interface connecting the upper and lower layers and **c** optical image of grain structure with the stacking of nearly parallel layers grown under the condition, ΔT = 60 °C and t_r = 5 mm/h

Similar kind of atomic packing due to the coalescence of two-dimensional islands giving evidence of layer-by-layer growth was observed by Kolesnikov et al. [28] in GaSe crystals. The laminated structure due to the propagation of close-packed planar interface, wherein the atomic layers are packed homogeneously, is depicted in Fig. 7a. Figure 7b is its schematic analogue, which illustrates the Kossel–Stranski–Volmer (KSV) model of growth [1, 25, 28]. As per this theoretical consideration, the growth units reaching the solid surface give up their kinetic energy and get deposited on the kinks leading to the tangential advancement of layers, inherent on its internal structure. If an atom leaves the molten liquid and joins the flat solid surface, its probability of attachment is much greater to kink sites in comparison with the ledge/steps in order to reduce the Gibbs free energy [29]. The development of crystals relies on the adsorption of atoms to the kinks and successive advancement of fairly straight steps, due to which a stack of symmetrical, parallel bands reflecting the route of crystallization was detected, as seen in Fig. 7c. Screw dislocation mechanism is ruled out as the helical features due to concentric spirals were not observed. Bulk crystallization was established by the continuance of surface steps leading to sequential deposition of layers. Repeated arrangement of growth bands within each crystal controls the microstructure by the virtue of regaining thermal stability. Atomic roughness of the interface was thus drastically reduced with decrease in translational rate

($\Delta T = 60$ °C and $t_r = 3$ mm/h), validating nearly perfect crystal growth as per the KSV model [21, 29, 32].

Furthermore, to obtain good quality crystals, the degree of departure from the equilibrium state was optimized with proper control of the driving force (supercooling), for which the crystallization temperature has to be scaled down very slowly. Thus to control the heat transfer, experiments were repeated by fine tuning t_r from 3 to 2 mm/h so as to boost the less dense binary system to undergo periodic atomic arrangement in accordance with the controlled movement of stable planar interface as shown in Fig. 1a and b, giving rise to densely packed crystals. Figure 8a depicts the formation of a flat crystalline surface. The results obtained for good quality SnSe crystals support the growth kinetics discussed in the literature [1, 21].

Higher supercooling led to enhanced driving force, attenuating the planar structure and inducing atomically rough surfaces (Fig. 8b, c) due to irregular atomic deposition [19]. Onset of polycrystallinity is vivid from these figures with imperfections.

3.2 Physical properties of SnSe crystals

As the properties are dependent on the microstructure of synthesized tin selenide crystals for device applications, it is vital to assess the presence of impurity elements, defects, etc. so as to enhance the mechanical strength, structural stability, optical band gap, etc. Therefore, the harvested
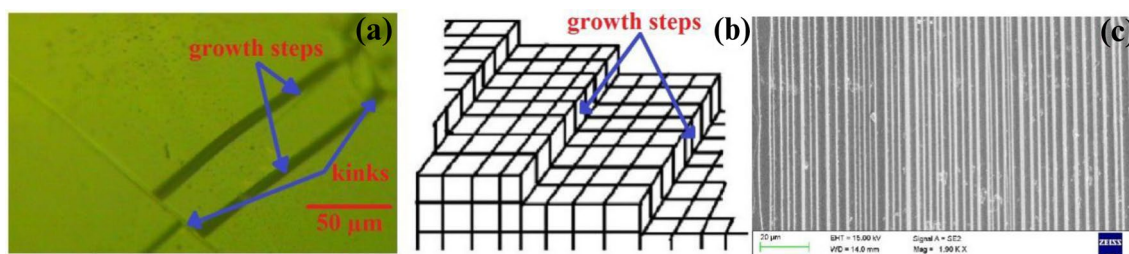
Fig. 7 **a** Optical image showing the formation of parallel steps ($\Delta T = 60$ °C and $t_r = 4$ mm/h), **b** Schematic diagram of a parallel stepped surface and **c** SEM image showing the formation of layer-by-layer growth ($\Delta T = 60$ °C and $t_r = 3$ mm/h)
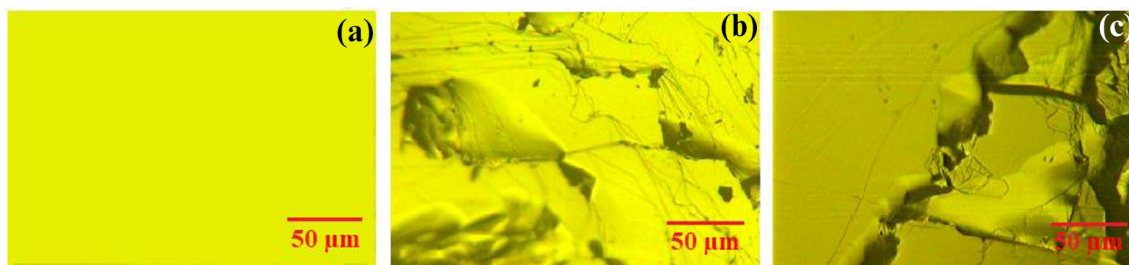

Fig. 8 Optical images of crystals grown under the conditions: **a** smooth surface, $\Delta T = 60$ °C and $t_r = 2$ mm/h, **b** rough surface, $\Delta T = 80$ °C and $t_r = 2$ mm/h and **c** $\Delta T = 100$ °C and $t_r = 2$ mm/h

products were subjected to EDAX analysis for testing the elemental analysis. Due to thermal asymmetry and oscillations, compositional alterations were dominant for $\Delta T = 100$ °C and as a result, tin rich samples containing only 47.93 at.% of selenium (Fig. 9) were obtained, disrupting the right chemical proportions. These non-stoichiometric samples resulting from constitutional supercooling bearing undesirable microstructures were not considered for further studies, as the non-homogeneity induce detrimental conditions for device quality improvement.

However, the chemical composition of Sn and Se in the crystals grown under the optimized conditions, $\Delta T = 60$ °C and $t_r = 2$ mm/h was found to be 50.01 and 49.99 at.% respectively, which agrees fairly well with the ideal stoichiometry, confirming the homogeneity of SnSe as evident from Fig. 10a. Spikes due to traces of oxygen were not observed, justifying the absence of oxidation. The estimated lattice parameters ($a = 4.446$ Å, $b = 11.502$ Å and $c = 4.152$ Å) are consistent with standard ICSD data (PDF-Number: 01-075-1843 48-1224). The sharpness of X-ray diffraction peaks justifies low lattice distortion and enhanced periodicity [33]. The indexed planes (Fig. 10b) manifest the orthorhombic
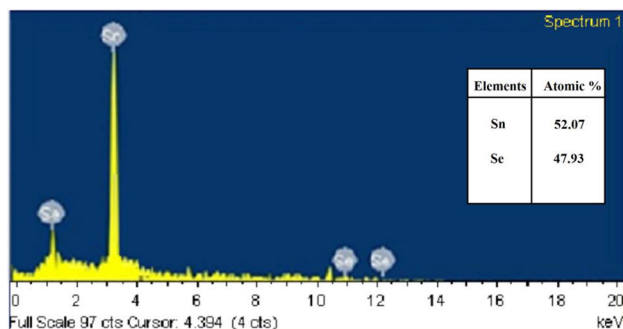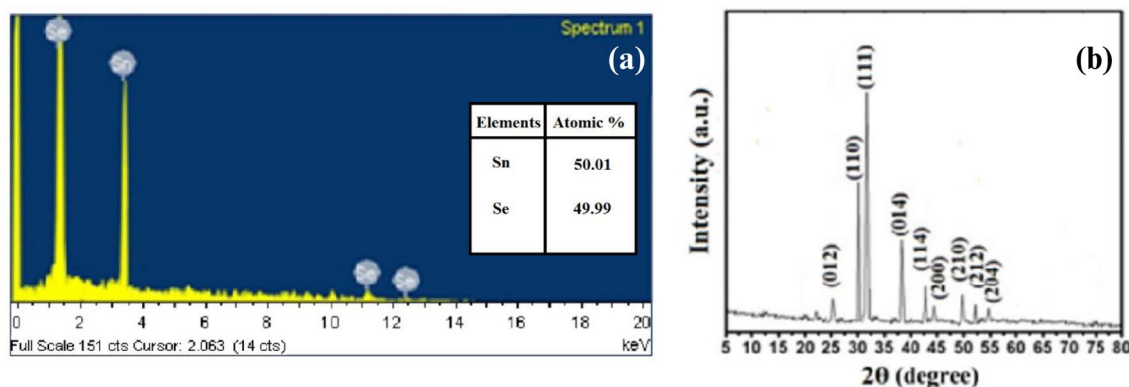
crystal system of SnSe layered samples. No other diffraction peaks belonging to any other phases were detected, eliminating the possibility of polymorphism. The estimated value of density using the experimental procedure based on the Archimedes principle is equal to 6.186 g/cm^3, which is in agreement with the reported ICSD crystallographic data. This result is comparable to that computed using the cell dimensions and molecular mass of the compound (6.183 g/cm^3). The research findings thus justify the right elemental proportion, single phase formation and crystal structure of the grown crystals, with the precise chemical homogeneity of tin and selenium, as established by the EDAX and PXRD analyses.

Thermogravimetric analysis (TGA) was carried out using a Perkin Elmer Model at a scanning range 15 °C to 1000 °C, under nitrogen atmosphere and heating rate of 5 °C/min. The low temperature regime in the profile (Fig. 11a) is found to be fairly linear. The sample began melting corresponding to a temperature ~ 860 °C (T_m), validating the right crystallization behaviour of SnSe in monophase system [34]. The thermal characteristics of the present SnSe crystals did not exhibit substantial structural changes before the melting point, but reported for their counterparts grown by the direct vapour transport [35]. The former rules out the existence of undesirable peaks, suggesting the absence of nitrogen adsorption. Continuous weight loss due to the dissociation of SnSe and loss of volatile selenium is commonly occurred for vapour growth from diluted or less dense gaseous phase as discussed by Sunagawa [19] and Agarwal et al. [35], but it has not been detected in the present case, confirming the homogeneity in chemical composition and thermal stability of the melt grown dense SnSe crystals, devoid of multiphases like $SnSe_2$, Sn_2Se_3, etc.

Microindentation analysis of a sample is essential to unearth the material strength and stability for device applications. Precise control of supercooling and growth velocity by eliminating undesirable features like globules,
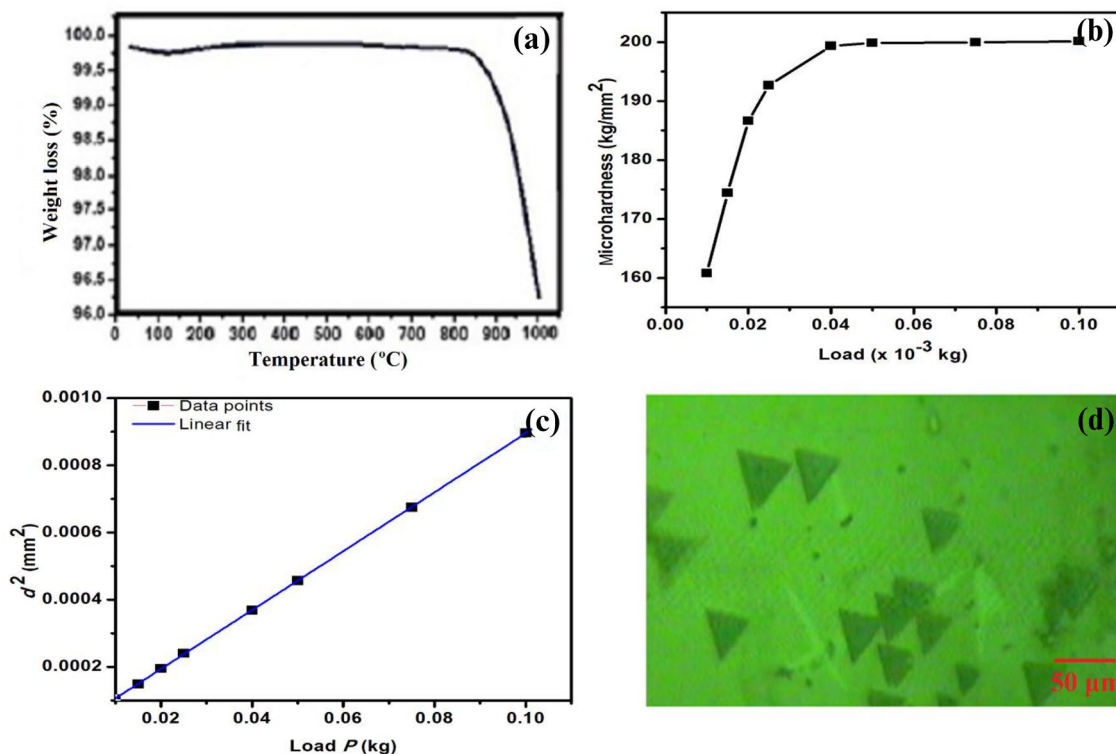

Fig. 9 EDAX profile of Sn rich crystal grown under the condition, $\Delta T = 100$ °C and $t_r = 2$ mm/h

Fig. 10 **a** EDAX profile and **b** XRD pattern of stoichiometric SnSe crystals grown under the condition, $\Delta T = 60$ °C and $t_r = 2$ mm/h

Fig. 11 **a** TGA profile **b** Plot of microhardness versus load **c** Variation of d^2 with applied load P and **d** Microscopic image of etch pits (600×)

flakes, voids, mounds, etc. attenuated plastic deformation and hence led to good mechanical stability of the melt grown SnSe crystals. The response to deformation on the crystal surface was investigated with respect to the effect of applied load (P) in the range, 10 to 100 g (Fig. 11b). Vickers microhardness, Hv, a measure of the ratio of load to the surface area of indentation mark, was computed based on the formula,

$$Hv = 2P \sin(\theta/2)/d^2, \tag{4}$$

where P is the load applied on the surface of the material, d is the mean diagonal length of the impression mark during indentation and θ is the angle between opposite faces of the pyramidal indenter (136°). The Meyer's index number (n), which relates the load and indentation diagonal length, was calculated based on the relation,

$$P = kd^n, \tag{5}$$

where k is the material constant. The straight line (Fig. 11c) connecting d^2 versus P passes through the origin, which indicates that error in loading is negligible in the studied range, validating Meyer's law. Elastic stiffness constant (C_H) was evaluated using the Wooster's empirical formula, log $C_H = 7/4 \log H_V$ [36], where C_H and H_V are proportional to each other. The values of yield strength were also calculated and presented in Table 2.

Table 2 Mechanical parameters of melt grown SnSe crystals

Load (kg)	Hardness (kg/mm^2)	Yield strength (kg/mm^2)	Stiffness constant (kg/mm^2)
0.010	160.81	53.60	7261.86
0.015	174.44	58.15	8372.99
0.020	186.63	62.21	9423.62
0.025	192.67	64.22	9963.79
0.040	199.32	66.44	10,573.38
0.050	199.82	66.61	10,619.84
0.075	199.94	66.65	10,631.01
0.100	200.13	66.71	10,648.69

The Young's modulus (E) was estimated using the relation,

$$E = 3Y \tan \theta_s \exp\left[\left(\frac{3H_v}{2Y}\right) - 2\right] \tag{6}$$

where Y is the yield strength and θ_s is the semi-angle of the diamond pyramidal indenter. The value ranges from 50 to 61 GPa for loads 10–100 g, which are comparable to that reported for GaTe crystals [37]. In the present work, as SnSe crystals grew layer-by-layer with nearly perfect interatomic

binding devoid of screw dislocations, the mechanical parameters were increased with load and followed saturation beyond the threshold load, 40 g due to strong chemical bonding. To the best of our knowledge, such research findings were not earlier reported for tin monoselenide crystals. Quality of the grown crystals was assessed by chemical etching, as it is a facile process to examine the distribution of defects [38]. Figure 11d depicts the photograph of an etched crystal surface in the etchant comprising a mixture of iodine, sulphuric acid and methanol for 15 s, showing triangular pits. The dislocation density is found to be $3.93 \times 10^2 \, cm^{-2}$, which is remarkably lesser than that reported in the literature [34, 39]. Other defects such as grain boundaries, stacking faults etc., that could have induced row of etch pits were not detected in the grown crystals due to the attenuation of internal stresses related to the constraining of neighbouring regions associated with thermal gradient, and hence enhanced the mechanical parameters. In order to investigate the optical properties, absorption spectrum of the grown SnSe crystals was recorded in the wavelengths ranging from 200 to 1500 nm by employing a UV–Vis–NIR spectrophotometer (Varian, Cary 5000). The light energy (hυ) depends on absorption coefficient (α) as per the equation,

$$(\alpha h\upsilon)^2 = A\left(h\upsilon - E_g\right), \tag{7}$$

where A is an arbitrary constant and E_g denotes the energy gap. From the $(\alpha h\upsilon)^2$ versus hυ profile (Fig. 12a), the value of $E_g = 1.32$ eV, which is greater than that reported by the earlier researchers [40]. The enhanced band gap and typical direct transition nature of the present crystals are associated with the superior stoichiometry and crystallinity.

The photoluminescence spectrum (PL) is an indispensable surface sensitive tool to investigate the emission band structure, presence of defects and the optical parameters of a semiconductor. Therefore, the PL emission spectrum of SnSe crystal was recorded at room temperature by subjecting

to an excitation wavelength of 730 nm (Fig. 12b), which showed a sharp and intense peak at 943.28 nm. The computed band gap ~ 1.32 eV is in agreement with UV–Vis–NIR data. Moreover, the absence of defect luminescence suggests that the samples are devoid of foreign elements in accordance with EDAX and PXRD profiles, which justifies the versatility of samples. It is thus worthwhile to emphasize that the scientific investigations based on a scalable microstructural approach have the potential to develop good quality samples bearing novel optical characteristics for solar cell applications.

4 Conclusions

The influence of growth conditions for the microstructural development of SnSe crystals by controlling supercooling (ΔT = 20 to 100 °C) and growth velocity (12–2 mm/h), utilizing an indigenously fabricated Bridgman–Stockbarger furnace under high vacuum, has been investigated for the first time. The growth conditions by stabilizing ΔT = 60 °C and $t_r = 2$ mm/h, were found to be optimal for facilitating periodic stacking of atomic layers as per the KSV model, which were subjected for further characterization. The EDAX analysis confirmed that the grown crystals are stoichiometric, as the atomic percentage of Sn and Se is equal to 50.01 and 49.99 at.% respectively, which is close to the ideal composition of SnSe. Powder X-ray diffractogram confirmed the monophase nature manifesting orthorhombic crystal system. Based on the Archimedes principle, the density of crystals is found to be 6.186 g/cm³, which supports the PXRD data. The sharpness of peaks justifies improved crystallinity of the grown samples. Thermogravimetric and microindentation analyses reflected appreciable thermal stability and mechanical strength. The low value of dislocation density (3.93×10^2 cm⁻²) validates nearly perfect ordering of crystal structure. Absorption characteristics of SnSe crystals investigated by
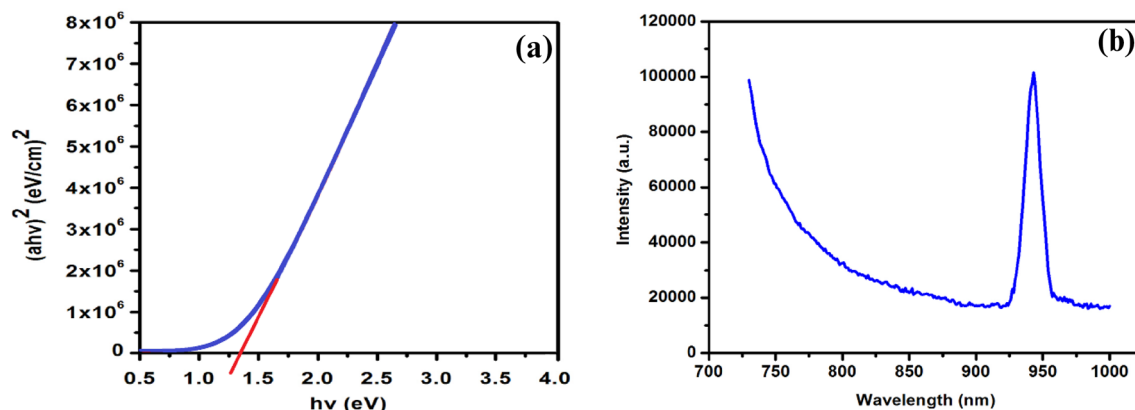
Fig. 12 **a** Plot of $(\alpha h\nu)^2$ versus photon energy and **b** PL spectrum of SnSe crystals

UV–Vis–NIR and PL showed direct transition nature with optimal band gap (1.32 eV) which mirror that the results are superior to those grown by other methods. SnSe crystalline structures engineered using a stoichiometric precursor are thus promising for the development of a suitable absorber material for solar energy harvesting applications.

References

1. H.J. Scheel, C. Peter, *Crystal Growth Technology: From Fundamentals and Simulation to Large-Scale Production* (Wiley, Hoboken, 2011)
2. B.R. Pamplin, *Crystal Growth* (Pergamon, Oxford, 1975)
3. S. Kasap, P. Capper, *Springer Handbook of Electronic and Photonic Materials* (Springer, New York, 2017)
4. T. Liu, P. Ge, W. Bi, P. Wang, Sol. Energy **157**, 427–433 (2017)
5. B. Terheiden, T. Ballmann, R. Horbelt, Y. Schiele, S. Seren, J. Ebser, G. Hahn, V. Mertens, M.B. Koentopp, M. Scherff, J.W. Müller, Phys. Status Solidi A **212**, 13–24 (2015)
6. M.A. Green, K. Emery, Y. Hishikawa, W. Warta, Prog. Photovolt. Res. Appl. **19**, 84–92 (2011)
7. G.H. Chandra, J.N. Kumar, N.M. Rao, S. Uthanna, J. Cryst. Growth **306**, 68–74 (2007)
8. H. Häberlin, *Photovoltaics: System Design and Practice* (Wiley, Hoboken, 2012)
9. M.R. Leys, H. Veenvliet, J. Cryst. Growth **55**, 145–153 (1981)
10. H.G.B. Hicks, D.F. Manley, Solid State Commun. **7**, 1463–1465 (1969)
11. W. Lee, M.C. Jeong, J.M. Myoung, Acta Mater. **52**, 3949–3957 (2004)
12. H. Li, W. Jie, J. Cryst. Growth **257**, 110–115 (2003)
13. B. Cao, W. Cai, J. Phys. Chem. C **112**, 680–685 (2008)
14. A.C. Bernardes-Silva, A.F. Mesquita, E. de Moura Neto, A.O. Porto, G.M. De Lima, J.D. Ardisson, F.S. Lameiras, Solid State Commun. **135**, 677–682 (2005)
15. A. Agarwal, J. Cryst. Growth **183**, 347–351 (1998)
16. J. Liu, Q. Huang, Y. Qian, Z. Huang, F. Lai, L. Lin, M. Guo, W. Zheng, Y. Qu, Cryst. Growth Des. **16**, 2052–2056 (2016)
17. A. Dahlen, A. Fattah, G. Hanke, E. Karthaus, Cryst. Res. Technol. **29**, 187–198 (1994)
18. H.L. Bhat, *Introduction to Crystal Growth: Principles and Practice* (CRC Press, Boca Raton, 2014)
19. I. Sunagawa, *Crystals: Growth, Morphology and Perfection* (Cambridge University Press, Cambridge, 2005)
20. R. Balasubramaniam, *Callister's Materials Science and Engineering* (Wiley, Hoboken, 2016)
21. D.A. Porter, K.E. Easterling, *Phase Transformations in Metals and Alloys* (Springer, New York, 1992)
22. V. Raghavan, *Materials Science and Engineering* (PHI Learning Private Limited, New Delhi, 2012)
23. P. Rudolph, M. Mühlberg, Mater. Sci. Eng. B **16**, 8–16 (1993)
24. M. Mühlberg, P. Rudolph, M. Laasch, E. Treser, J. Cryst. Growth **128**, 571–575 (1993)
25. Y.O. Kanter, Cryst. Res. Technol. **16**, 1333–1338 (1981)
26. I. Kikuma, M. Sekine, M. Furukoshi, J. Cryst. Growth **75**, 609–612 (1986)
27. M.R. Lorenz, J. Phys. Chem. Solids **23**, 939–947 (1962)
28. N.N. Kolesnikov, E.B. Borisenko, D.N. Borisenko, V.K. Gartman, J. Cryst. Growth **300**, 294–298 (2007)
29. M. Teena, A.G. Kunjomana, J. Appl. Crystallogr. **50**, 1125–1132 (2017)
30. J. Málek, J. Shánělová, S. Martinková, P. Pilný, P. Koštál, Cryst. Growth Des. **17**, 4990–4999 (2017)
31. J.C. Brice, E.P. Wohlfarth, *The Growth of Crystals From the Melt*, vol. 3 (North-Holland, Amsterdam, 1965)
32. I. Minkoff, B. Lux, J. Cryst. Growth **22**, 163–165 (1974)
33. H. Wiedemeier, H. Georg, G. von Schnering, Cryst. Mater. **148**, 295–304 (1978)
34. V.P. Bhatt, K. Gireesan, G.R. Pandya, J. Cryst. Growth **96**, 649–651 (1989)
35. A. Agarwal, P.D. Patel, D. Lakshminarayana, J. Cryst. Growth **142**, 344–348 (1994)
36. W.A. Wooster, Rep. Prog. Phys. **16**, 62 (1953)
37. A.G. Kunjomana, M. Teena, K.A. Chandrasekharan, J. Appl. Crystallogr. **47**, 1841–1848 (2014)
38. A. Senthil, P. Ramasamy, J. Cryst. Growth **401**, 200–204 (2014)
39. T.A. Campbell, M. Schweizer, P. Dold, A. Cröll, K.W. Benz, J. Cryst. Growth **226**, 231–239 (2001)
40. I. Lefebvre, M.A. Szymanski, J. Olivier-Fourcade, J.C. Jumas, Phys. Rev. B **58**, 1896 (1998)